JOURNAL OF CHEMICAL & ENGINEERING DATA

ARTICLE

pubs.acs.org/jced

CO_2 Absorption Rate into Concentrated Aqueous Monoethanolamine and Piperazine

Ross E. Dugas and Gary T. Rochelle*

Luminant Carbon Management Program, Department of Chemical Engineering, The University of Texas at Austin, 1 University Station C0400, Austin, Texas 78712, United States

ABSTRACT: The CO_2 equilibrium partial pressure and liquid film mass transfer coefficient (k_g') in (7, 9, 11, and 13) m monoethanolamine (MEA) and (2, 5, 8, and 12) m piperazine (PZ) were measured in a wetted wall column. Also examined was 7 m MEA/2 m PZ. Absorption and desorption experiments were performed at (40, 60, 80, and 100) °C over a range of CO_2 loading. Amine concentration does not affect the CO_2 partial pressure of PZ or MEA solutions as a function of CO_2 loading with less than 0.45 mols CO_2/mol alkalinity. Changes in amine concentration and temperature often do not affect the measured value of k_g'. At higher temperature and CO_2 loading in PZ, the diffusion of reactants and products limits CO_2 transfer, and k_g' is depressed. PZ (8 m) exhibits a 70 % greater CO_2 capacity than 7 m MEA and a 50 % greater CO_2 capacity than 11 m MEA. k_g' decreases by a factor of 30 in aqueous MEA with 0.23 to 0.50 CO_2 loading. k_g' decreases by a factor of 20 in aqueous PZ with 0.21 to 0.41 CO_2 loading. PZ is shown to absorb CO_2 2 to 3 times faster than MEA.

INTRODUCTION

Carbon capture from flue gas by absorption/stripping with aqueous amine will probably be an important technology with which to address global climate change. Aqueous monoethanolamine (MEA) at 7 m has been used at a smaller scale to remove CO_2 from flue gas and represents an important baseline technology. Concentrated piperazine[1] has been identified as a promising advanced solvent for this application. The rate of CO_2 absorption by these solvents is determined by diffusion with fast reaction in the liquid boundary layer.

Carbon dioxide (CO_2) absorption rate into monoethanolamine (MEA) has been measured by over 20 researchers.[2−7] CO_2 absorption rate in aqueous piperazine (PZ) has been measured by fewer researchers.[7−12] Most of the data have been obtained near ambient temperature with unloaded, dilute amine. Only Aboudheir provides MEA rate data at sufficiently high temperature, amine concentration, and CO_2 loading to effectively characterize industrial CO_2 capture systems. No large data source for concentrated aqueous PZ is available in the literature. This work provides MEA and PZ rate data at high amine concentration, typical CO_2 loading, and typical process temperature.

Historically, PZ has been viewed as a promoter since it reacts very fast with CO_2, but it has been perceived to have limited solubility.[1] Recent solid solubility data have shown that PZ has the capability to be used in very high concentrations when it is partially loaded with CO_2.[1,13] Aqueous piperazine systems have also shown a very high resistance to thermal degradation.[1,14]

CO_2 absorption/desorption rates were measured for (2, 5, 8, and 12) m (gmol·kg^{-1} water) PZ [(15 to 51) wt %] at (40 to 100) °C. As a comparison and supplement to the literature data, MEA was tested at (7, 9, 11, and 13) m [(30 to 44) wt %]. A 7 m MEA/2 m PZ solution was also analyzed, although this solution has shown poor thermal stability.[14] At each amine concentration, at least four CO_2 loadings were analyzed. The CO_2 loading was chosen to represent the range of expected lean and rich solution compositions present in an industrial CO_2 capture system.

CO_2 loading is reported on a mol_{CO2}/mol_{alk} basis. Since PZ has two active nitrogen groups per molecule, it has 2 mol of alkalinity per mole of PZ. Monoethanolamine and PZ structures are shown in eqs 1 and 2. The CO_2 loading definition is shown in eq 3.

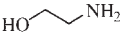

(1)

(2)

$$\text{CO}_2\text{ loading} = \frac{n_{CO2}}{n_{MEA} + 2n_{PZ}} \quad (3)$$

EXPERIMENTAL METHODS

CO_2 equilibrium partial pressure and CO_2 absorption/desorption rate were measured in a wetted wall column originally constructed by Mshewa.[15] Various researchers have used this wetted wall column to collect rate and equilibrium partial pressure data.[4,8,15−18] A schematic of the entire apparatus is shown in Figure 1. A closer view of the reaction chamber is shown in Figure 2. Details of the exact dimensions are also available.[19]

Received: November 16, 2010
Accepted: March 31, 2011
Published: April 19, 2011

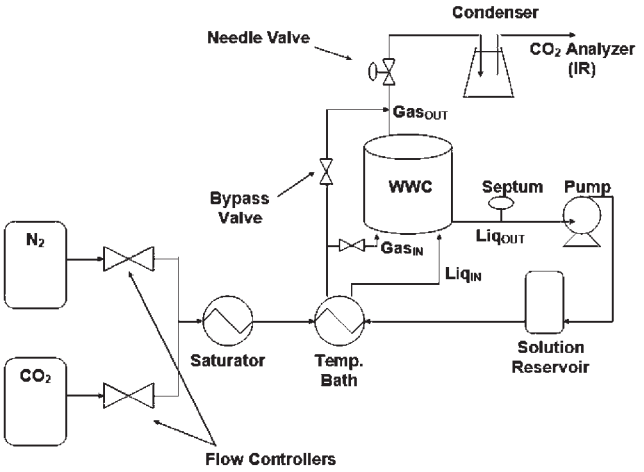

Figure 1. Schematic diagram of the wetted wall column apparatus.

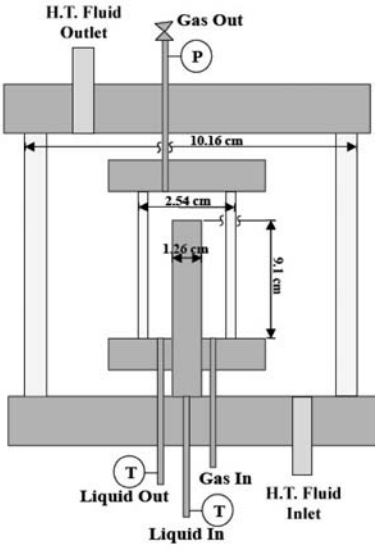

Figure 2. Detailed view of the wetted wall column reaction chamber.

Nitrogen and carbon dioxide flows (each 0 to 5 SLPM) are controlled by mass flow controllers to create a simulated flue gas of known concentration. The N_2/CO_2 blend is routed to a saturator which consists of a fritted bubbler under (8 to 10) in. of water surrounded by an oil bath. The gas is then passed through tubing immersed in another temperature bath. The gas enters the wetted wall column, and CO_2 is either absorbed or desorbed by the solvent. The exit gas is routed through a flask immersed in an ice bath before being sent through a desiccant to a Horiba VIA-510 CO_2 analyzer.

Unlike the gas, the solution is recycled through the system. The system was operated with about 2.2 L of solution. The screw-type positive displacement pump can be controlled to circulate liquid rates of (2 to 4) $mL \cdot s^{-1}$. Liquid rates are observed by a simple rotameter.

The gas−liquid interface occurs on the perimeter of the 9.1 cm tall stainless steel tube. The solution flows upward through the borehole and overflows down the perimeter of the tube. The upward-flowing gas and the downward-flowing liquid contact each other, and CO_2 mass transfer is achieved over the known surface area of the tube. The wetted area is 38.52 cm^2 (assuming a hemisphere of liquid is present above the borehole). The annular region for gas flow and the inside diameter of the cell are estimated to be 1.30 cm^2 and 1.70 cm.[17]

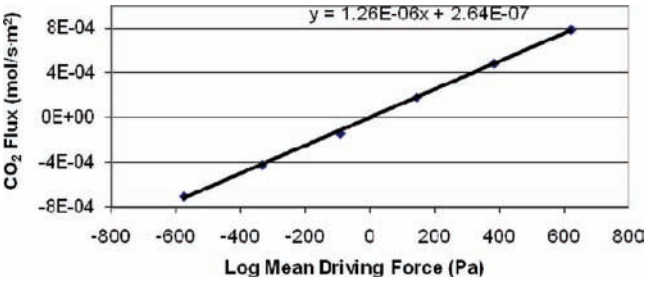

Figure 3. Flux against log mean driving force plot for 7 m MEA, 0.351 loading, 60 °C.

Due to the nature of the wetted wall column experiments, experimental conditions were adjusted over a large range of pressures [(15 to 70) psig] and flow rates (3 to 5 SLPM) to maximize data quality.

Amine solutions were prepared gravimetrically. CO_2 was added to the solvent using a bubbler column with a glass frit. The column was placed on a scale. As CO_2 dissolved into the liquid phase and reacted with amine, the additional mass of CO_2 was recorded by the scale. The CO_2 loading of the solution was officially determined using a total inorganic carbon method. Solvent was injected into 30 wt % phosphoric acid. A nitrogen carrier gas bubbling through the acid sweeps away liberated CO_2 and passes it through a magnesium perchlorate desiccant before analysis by a PIR-2000 infrared analyzer.

DATA INTERPRETATION

Generally, six experimental inlet CO_2 partial pressures were examined in the wetted wall column for each solvent composition at a given temperature. The six pressures were chosen so that half were expected to result in absorption, while the other three yielded CO_2 desorption from the solvent. Performing absorption and desorption experiments and measuring CO_2 fluxes allows for a very accurate determination of the CO_2 partial pressure.

The flux of CO_2 into or out of the solvent is directly proportional to the CO_2 driving force between the partial pressure of CO_2 in the gas phase and the equilibrium partial pressure of CO_2 exerted by the solvent. Although the equilibrium partial pressure is not explicitly measured, it can be determined by plotting the flux versus the log mean driving force as shown in Figure 3. The equilibrium partial pressure, $P^*_{CO2,b}$, used in the log mean driving force calculation is adjusted until the trend line passes through the origin. This zero flux condition defines the equilibrium partial pressure. The slope of the line in Figure 3 corresponds to the overall mass transfer coefficient, K_G.

$$N_{CO2} = K_G(P_{CO2} - P^*_{CO2,b}) \quad (4)$$

The overall mass transfer coefficient, K_G, is both a function of the apparatus geometry (gas phase mass transfer) and the solvent mass transfer properties. Although solvent reaction rates are reported in terms of k_g', k_g' can be subdivided into kinetic and physical mass transfer resistances. Equation 5 shows the correlation between all the mass transfer coefficients. The slope of the equilibrium line results from changing a concentration driving

Table 1. CO_2 Equilibrium Partial Pressure and Rate Data Obtained from the Wetted Wall Column with Aqueous MEA

MEA		T	liquid CO_2		k_l^o	P^*_{CO2}	k_g'
m	x	°C	mol/mol$_{alk}$	x	m·s^{-1}	Pa	mol·s^{-1}·Pa^{-1}·m^{-2}
7	0.109	40	0.252	0.027	$7.5\cdot10^{-5}$	15.7	$3.34\cdot10^{-6}$
	0.108		0.351	0.038	$6.4\cdot10^{-5}$	77	$1.40\cdot10^{-6}$
	0.107		0.432	0.046	$6.3\cdot10^{-5}$	465	$7.66\cdot10^{-7}$
	0.106		0.496	0.053	$6.5\cdot10^{-5}$	4216	$3.47\cdot10^{-7}$
	0.109	60	0.252	0.027	$9.0\cdot10^{-5}$	109	$2.92\cdot10^{-6}$
	0.108		0.351	0.038	$8.0\cdot10^{-5}$	660	$1.70\cdot10^{-6}$
	0.107		0.432	0.046	$7.9\cdot10^{-5}$	3434	$9.28\cdot10^{-7}$
	0.106		0.496	0.053	$7.9\cdot10^{-5}$	16157	$3.76\cdot10^{-7}$
	0.109	80	0.271	0.029	$9.7\cdot10^{-5}$	1053	$2.85\cdot10^{-6}$
	0.107		0.366	0.039	$8.6\cdot10^{-5}$	4443	$1.87\cdot10^{-6}$
	0.109	100	0.271	0.029	$1.1\cdot10^{-4}$	5297	$2.98\cdot10^{-6}$
	0.109		0.366	0.039	$9.6\cdot10^{-5}$	19008	$1.40\cdot10^{-6}$
9	0.135	40	0.231	0.031	$7.2\cdot10^{-5}$	10.4	-
	0.133		0.324	0.043	$6.3\cdot10^{-5}$	34	$1.86\cdot10^{-6}$
	0.132		0.382	0.051	$6.1\cdot10^{-5}$	107	$1.40\cdot10^{-6}$
	0.131		0.441	0.058	$5.9\cdot10^{-5}$	417	$8.36\cdot10^{-7}$
	0.130		0.496	0.065	$5.9\cdot10^{-5}$	5354	$3.02\cdot10^{-7}$
	0.135	60	0.231	0.031	$8.3\cdot10^{-5}$	61	$3.80\cdot10^{-6}$
	0.133		0.324	0.043	$7.7\cdot10^{-5}$	263	$2.44\cdot10^{-6}$
	0.132		0.382	0.051	$7.4\cdot10^{-5}$	892	$1.47\cdot10^{-6}$
	0.131		0.441	0.058	$7.3\cdot10^{-5}$	2862	$9.57\cdot10^{-7}$
	0.130		0.496	0.065	$7.0\cdot10^{-5}$	21249	$3.24\cdot10^{-7}$
	0.134	80	0.265	0.036	$8.9\cdot10^{-5}$	979	$3.24\cdot10^{-6}$
	0.133		0.356	0.047	$9.2\cdot10^{-5}$	4797	$1.75\cdot10^{-6}$
	0.134	100	0.265	0.036	$9.7\cdot10^{-5}$	4940	$3.40\cdot10^{-6}$
	0.133		0.356	0.047	$1.0\cdot10^{-4}$	21534	$1.33\cdot10^{-6}$
11	0.158	40	0.261	0.041	$6.0\cdot10^{-5}$	14.0	$3.36\cdot10^{-6}$
	0.156		0.353	0.055	$5.5\cdot10^{-5}$	67	$1.76\cdot10^{-6}$
	0.154		0.428	0.066	$5.2\cdot10^{-5}$	434	$7.14\cdot10^{-7}$
	0.154		0.461	0.071	$5.1\cdot10^{-5}$	1509	$4.34\cdot10^{-7}$
	0.158	60	0.261	0.041	$7.4\cdot10^{-5}$	96	$3.35\cdot10^{-6}$
	0.156		0.353	0.055	$6.7\cdot10^{-5}$	634	$1.80\cdot10^{-6}$
	0.154		0.428	0.066	$6.4\cdot10^{-5}$	3463	$8.71\cdot10^{-7}$
	0.154		0.461	0.071	$6.3\cdot10^{-5}$	8171	$5.02\cdot10^{-7}$
	0.159	80	0.256	0.041	$9.1\cdot10^{-5}$	860	$4.35\cdot10^{-6}$
	0.156		0.359	0.056	$8.2\cdot10^{-5}$	3923	$1.93\cdot10^{-6}$
	0.159	100	0.256	0.041	$1.0\cdot10^{-4}$	4274	$3.72\cdot10^{-6}$
	0.156		0.359	0.056	$9.1\cdot10^{-5}$	18657	$1.56\cdot10^{-6}$
13	0.181	40	0.252	0.046	$5.4\cdot10^{-5}$	12.3	$3.08\cdot10^{-6}$
	0.177		0.372	0.066	$4.7\cdot10^{-5}$	84	$1.28\cdot10^{-6}$
	0.175		0.435	0.076	$4.7\cdot10^{-5}$	491	$6.96\cdot10^{-7}$
	0.173		0.502	0.087	$4.5\cdot10^{-5}$	8792	$1.62\cdot10^{-7}$
	0.181	60	0.252	0.046	$6.4\cdot10^{-5}$	100	$2.98\cdot10^{-6}$
	0.177		0.372	0.066	$5.8\cdot10^{-5}$	694	$1.54\cdot10^{-6}$
	0.175		0.435	0.076	$5.7\cdot10^{-5}$	3859	$7.56\cdot10^{-7}$
	0.173		0.502	0.087	$5.5\cdot10^{-5}$	29427	$1.93\cdot10^{-7}$
	0.181	80	0.254		$8.3\cdot10^{-5}$	873	$4.21\cdot10^{-6}$
	0.178		0.355		$7.5\cdot10^{-5}$	3964	$1.85\cdot10^{-6}$
	0.181	100	0.254		$9.2\cdot10^{-5}$	3876	$3.66\cdot10^{-6}$
	0.178		0.355		$8.3\cdot10^{-5}$	18406	$1.56\cdot10^{-6}$

force to a partial pressure driving force to enable a series resistance relationship with K_G, k_g, and k_g''.

$$\frac{1}{K_G} = \frac{1}{k_g} + \frac{1}{k_g'} = \frac{1}{k_g} + \frac{1}{k_g''} + \frac{1}{k^o_{l,prod}}\left(\frac{\Delta P^*_{CO2}}{\Delta[CO_2]}\right) \quad (5)$$

Pacheco[17] quantified the gas film mass transfer coefficient, k_g, for the wetted wall column using a dimensional analysis approach. He quantified the physical liquid film mass transfer coefficient, k_l^o, of the wetted wall column using a theoretical model approach. The model solves the continuity equation for diffusion into a falling liquid film where convective transport is considered in the direction of the flow, while diffusive transport is considered in the direction perpendicular to the gas−liquid interface. Equations 6 to 8 quantify the physical mass transfer coefficients in the wetted wall column.

$$Sh = 1.075\left[ReSc\left(\frac{d}{h}\right)\right]^{0.85} \quad (6)$$

$$Sh = \frac{RTk_g d}{D_{CO2}} \quad (7)$$

$$k^o_{l,CO_2} = \left(\frac{3^{1/3}2^{1/2}}{\pi^{1/2}}\right)\left(\frac{Q^{1/3}h^{1/2}W^{2/3}}{A}\right)\left(\frac{g\rho}{\mu}\right)^{1/6} D^{1/2}_{CO2} \quad (8)$$

Greater detail on data interpretation to determine the equilibrium partial pressure and k_g' is referenced by Dugas.[19]

The methods for measurement of CO_2 loading and CO_2 partial pressure are ± 5 %. Measurements of k_g' and k_l^o are ± 10 %. Temperature measurements are ± 1 K.

RESULTS AND DISCUSSION

Experimental Data. Tables 1 to 3 provide tabulated data on the CO_2 transfer rate and the equilibrium CO_2 partial pressure. The liquid phase mole fractions, x, of amine and CO_2 have been calculated assuming that the solution composition is reported as total amine, total CO_2, and water. The rate data are given as k_g', defined as the liquid film mass transfer coefficient with a partial pressure driving force (eq 9). $P_{CO2,i}$ and $P^*_{CO2,b}$ refer to the CO_2 partial pressure at the gas−liquid interface and the bulk liquid.

$$k_g' = \frac{N_{CO2}}{(P_{CO2,i} - P^*_{CO2,b})} \quad (9)$$

Each row of Tables 1 to 3 represents the result of six experimental inlet CO_2 partial pressures. Much more detailed data including flow rates, pressures, and inlet and outlet CO_2 partial pressures and gas film resistance have been reported.[19] Some experiments, particularly PZ experiments, seem to be limited by the diffusion of reactants and products near the interface. Therefore, $k^0_{l,prod}$ is also reported in Tables 1 and 2.

PZ experiments (12 m) at 40 °C could not be run in the wetted wall column due to the high viscosity of the solution. PZ samples (12 m) with approximately 0.40 CO_2 loading were not tested due to solubility limitations.

Equilibrium CO_2 Partial Pressure and Literature Comparisons. Figure 4 shows equilibrium CO_2 partial pressure obtained with the wetted wall column for (7, 9, 11, and 13) m MEA

Table 2. CO_2 Equilibrium Partial Pressure and Rate Data Obtained from the Wetted Wall Column with Aqueous PZ

PZ		T	liquid CO_2		k'	P^*_{CO2}	k_g'
m	x	°C	mol/mol$_{alk}$	x	m·s^{-1}	Pa	mol·s^{-1}·Pa^{-1}·m^{-2}
2	0.034	40	0.240	0.016	$9.0\cdot10^{-5}$	96	$3.32\cdot10^{-6}$
	0.034		0.316	0.021	$9.0\cdot10^{-5}$	499	$2.04\cdot10^{-6}$
	0.034		0.352	0.024	$8.9\cdot10^{-5}$	1305	$1.39\cdot10^{-6}$
	0.034		0.411	0.028	$9.0\cdot10^{-5}$	7127	$5.55\cdot10^{-7}$
	0.034	60	0.240	0.016	$1.1\cdot10^{-4}$	559	$3.33\cdot10^{-6}$
	0.034		0.316	0.021	$1.1\cdot10^{-4}$	2541	$2.06\cdot10^{-6}$
	0.034		0.352	0.024	$1.1\cdot10^{-4}$	5593	$1.38\cdot10^{-6}$
	0.034		0.411	0.028	$1.0\cdot10^{-4}$	25378	$3.84\cdot10^{-7}$
	0.034	80	0.239	0.016	$1.3\cdot10^{-4}$	2492	$3.34\cdot10^{-6}$
	0.034		0.324	0.022	$1.3\cdot10^{-4}$	12260	$1.32\cdot10^{-6}$
	0.034	100	0.239	0.016	$1.5\cdot10^{-4}$	9569	$2.40\cdot10^{-6}$
	0.034		0.324	0.022	$1.5\cdot10^{-4}$	39286	$9.12\cdot10^{-7}$
5	0.080	40	0.226	0.036	$6.0\cdot10^{-5}$	65	$4.39\cdot10^{-6}$
	0.079		0.299	0.047	$5.7\cdot10^{-5}$	346	$2.57\cdot10^{-6}$
	0.078		0.354	0.055	$5.4\cdot10^{-5}$	1120	$1.69\cdot10^{-6}$
	0.077		0.402	0.062	$5.3\cdot10^{-5}$	4563	$7.93\cdot10^{-7}$
	0.080	60	0.226	0.036	$7.4\cdot10^{-5}$	385	$4.75\cdot10^{-6}$
	0.079		0.299	0.047	$7.0\cdot10^{-5}$	1814	$2.62\cdot10^{-6}$
	0.078		0.354	0.055	$6.6\cdot10^{-5}$	5021	$1.80\cdot10^{-6}$
	0.077		0.402	0.062	$6.2\cdot10^{-5}$	17233	$6.59\cdot10^{-7}$
	0.079	80	0.238	0.038	$8.8\cdot10^{-5}$	2192	$4.67\cdot10^{-6}$
	0.078		0.321	0.050	$8.1\cdot10^{-5}$	9699	$1.91\cdot10^{-6}$
	0.079	100	0.238	0.038	$9.6\cdot10^{-5}$	8888	$3.52\cdot10^{-6}$
	0.078		0.321	0.050	$9.0\cdot10^{-5}$	36960	$1.02\cdot10^{-6}$
8	0.119	40	0.231	0.055	$3.8\cdot10^{-5}$	68	$4.27\cdot10^{-6}$
	0.117		0.305	0.071	$3.5\cdot10^{-5}$	530	$1.98\cdot10^{-6}$
	0.115		0.360	0.083	$3.7\cdot10^{-5}$	1409	$1.14\cdot10^{-6}$
	0.114		0.404	0.092	$3.6\cdot10^{-5}$	8153	$3.53\cdot10^{-7}$
	0.119	60	0.231	0.055	$5.1\cdot10^{-5}$	430	$4.41\cdot10^{-6}$
	0.117		0.305	0.071	$4.7\cdot10^{-5}$	2407	$2.02\cdot10^{-6}$
	0.115		0.360	0.083	$4.7\cdot10^{-5}$	7454	$9.57\cdot10^{-7}$
	0.114		0.404	0.092	$4.6\cdot10^{-5}$	30783	$3.20\cdot10^{-7}$
	0.118	80	0.253	0.060	$6.0\cdot10^{-5}$	3255	$3.61\cdot10^{-6}$
	0.117		0.289	0.068	$5.8\cdot10^{-5}$	9406	$1.97\cdot10^{-6}$
	0.118	100	0.253	0.060	$6.7\cdot10^{-5}$	13605	$2.18\cdot10^{-6}$
	0.117		0.289	0.068	$6.4\cdot10^{-5}$	32033	$1.20\cdot10^{-6}$
12	0.164	60	0.231	0.076	$3.6\cdot10^{-5}$	331	$4.19\cdot10^{-6}$
	0.161		0.289	0.093	$3.4\cdot10^{-5}$	1865	$1.85\cdot10^{-6}$
	0.158		0.354	0.112	$3.1\cdot10^{-5}$	6791	$7.73\cdot10^{-7}$
	0.165	80	0.222	0.073	$7.2\cdot10^{-5}$	2115	$4.24\cdot10^{-6}$
	0.161		0.290	0.093	$4.1\cdot10^{-5}$	9141	$1.48\cdot10^{-6}$
	0.165	100	0.222	0.073	$8.0\cdot10^{-5}$	7871	$3.78\cdot10^{-6}$
	0.161		0.290	0.093	$4.6\cdot10^{-5}$	33652	$8.30\cdot10^{-7}$

compared to Jou[20] and Hilliard.[13] Hilliard used an equilibrium cell to measure CO_2 partial pressure with an FTIR (Fourier transform infrared spectroscopy) analyzer to quantify the CO_2 concentration. Jou measured the equilibrium partial pressure with an equilibrium cell. This semibatch process adds additional CO_2 to a cell containing amine solution with a vapor headspace until pressure is stabilized at a predetermined value.

Table 3. CO_2 Equilibrium Partial Pressure and Rate Data Obtained from the Wetted Wall Column with 7 m MEA/2 m PZ

MEA		PZ		T	liquid CO_2		P^*_{CO2}	k_g'
m	x	m	x	°C	mol/mol$_{alk}$	x	Pa	mol·s^{-1}·Pa^{-1}·m^{-2}
7	0.104	2	0.03	40	0.242	0.04	27	$3.45\cdot10^{-6}$
	0.103		0.029		0.333	0.054	166	$1.96\cdot10^{-6}$
	0.101		0.029		0.416	0.066	1425	$8.76\cdot10^{-7}$
	0.100		0.029		0.477	0.075	7418	$4.32\cdot10^{-7}$
	0.104		0.03	60	0.242	0.04	178	$4.00\cdot10^{-6}$
	0.103		0.029		0.333	0.054	1256	$2.03\cdot10^{-6}$
	0.101		0.029		0.416	0.066	7122	$9.08\cdot10^{-7}$
	0.100		0.029		0.477	0.075	33704	$3.75\cdot10^{-7}$
	0.104		0.03	80	0.242	0.04	1138	$4.29\cdot10^{-6}$
	0.103		0.029		0.333	0.054	6174	$2.12\cdot10^{-6}$
	0.104		0.03	100	0.242	0.04	4340	$4.83\cdot10^{-6}$
	0.103		0.029		0.333	0.054	26571	$1.23\cdot10^{-6}$

When P_{CO2} is plotted as a function of loading, all of the data with the wetted wall column and the literature data fall on the same curve at each T up to a loading of about 0.45. At greater loading P^*_{CO2} appears to increase with MEA concentration, and the values from the wetted wall column are greater than those from Hilliard or Jou. The effect of MEA concentration on the CO_2 partial pressure is probably due to significant bicarbonate at the greater loading. Reaction stoichiometry suggests that carbamate formation should be independent of the total amine concentration, while bicarbonate formation should not.[19] The disagreement of data at greater loading from the difference sources probably results from the difficulties in sampling and analyzing the rich solutions with high CO_2 partial pressure.

Figure 5 shows equilibrium CO_2 partial pressure measured by the wetted wall column with (2, 5, 8, and 12) m PZ compared to Ermatchkov[21] and Hilliard.[13] Hilliard used an equilibrium cell to measure CO_2 partial pressure with an FTIR analyzer to quantify the CO_2 concentration. Ermatchkov measured the equilibrium partial pressure using headspace gas chromatography.[22]

All the data in Figure 5 match very well at (40, 60, and 80) °C. Neither Ermatchkov[21] nor Hilliard[13] provide data at 100 °C, but the 100 °C data look reliable based on the spacing from the 80 °C data and the overlap of the amine concentrations.

Very few data for equilibrium CO_2 partial pressure are available for 7 m MEA/2 m PZ. Figure 6 includes the current data compared against measurements by Hilliard.[13]

Although there are limited data for 7 m MEA/2 m PZ, the available equilibrium CO_2 partial pressure data show a very good match despite using two very different experimental methods.

CO_2 Capacity. The equilibrium CO_2 partial pressures in Figures 4 to 6 allow for the determination of the CO_2 capacity of the systems (Figure 7). The CO_2 capacity is defined as the difference in the CO_2 concentration in the rich and lean amine streams, essentially the amount of CO_2 that would be removed from the system during a circulation of the amine solution. CO_2 capacities are calculated as mol$_{CO2}$/kg(water + amine). It is not convenient to include the CO_2 in the weight of the solution since it has a mostly negligible sensible heat. Essentially, a mole of MEA has almost the same heat capacity as MEA carbamate.[13] Nguyen has seen the same effect in PZ systems.[23]

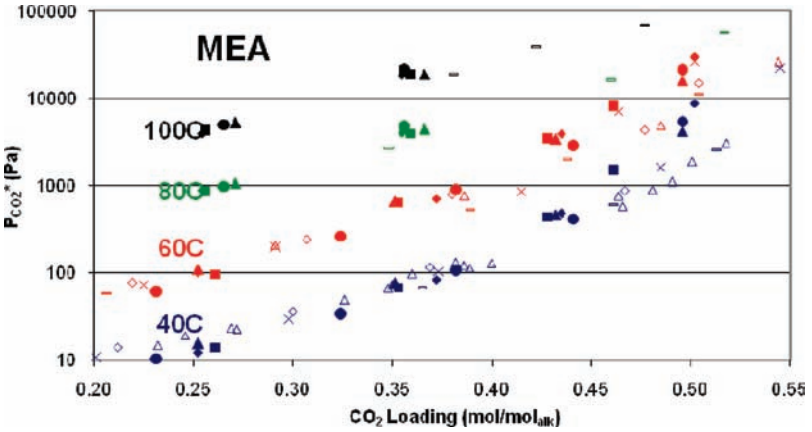

Figure 4. Equilibrium CO_2 partial pressure in MEA measured in the wetted wall column at (40, 60, 80, and 100) °C compared to literature (current work: 7 m MEA (▲), 9 m MEA (●), 11 m MEA (■), 13 m MEA (♦); Hilliard:[12] 3.5 m MEA (◊), 7 m MEA (△), 11 m MEA (×); Jou et al.:[19] 7 m MEA (−)).

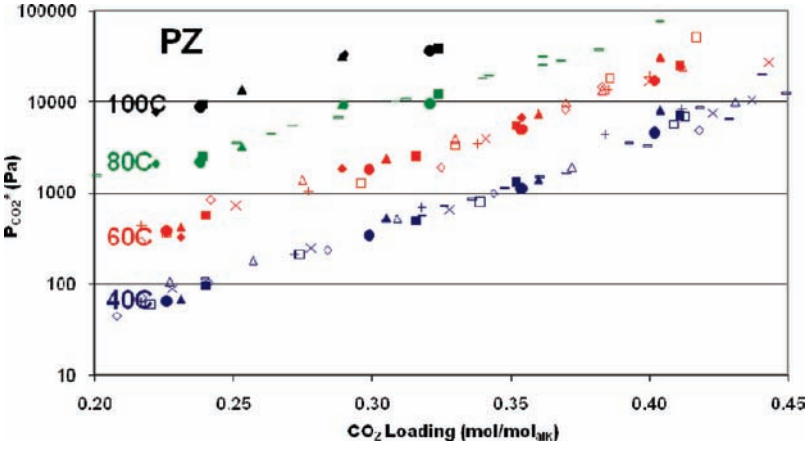

Figure 5. Equilibrium CO_2 partial pressure measurements in PZ solutions at (40, 60, 80, and 100) °C (Current work: 2 m PZ (■), 5 m PZ (●), 8 m PZ (▲), 12 m PZ (♦); Ermatchkov et al.:[20] 1−4.2 m PZ (−); Hilliard:[12] 0.9 m PZ (◊), 2 m PZ (△), 2.5 m PZ (×), 3.6 m PZ (+), 5 m PZ (□)).

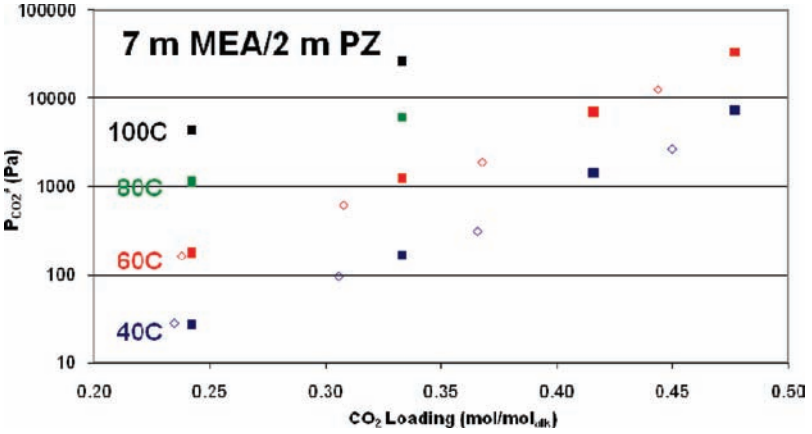

Figure 6. Equilibrium CO_2 partial pressure measurements in 7 m MEA/2 m PZ at (40, 60, 80, and 100) °C (Current work: (■); Hilliard:[12] (◊)).

The assumption of a 5 kPa CO_2 partial pressure rich solution at 40 °C represents a 5/12 or 42 % approach to saturation at the bottom of the absorber if the solution exits at 40 °C and encounters 12 % CO_2 flue gas. PZ (8 m) exhibits 70 % greater CO_2 capacity than 7 m MEA and 50 % greater CO_2 capacity than 11 m MEA. The majority of this increased CO_2 capacity is due to the fact that each mole of PZ has two functional nitrogen groups while MEA only has one.

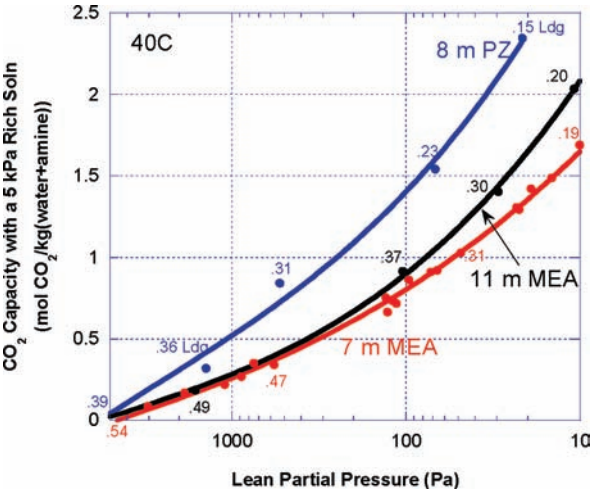

Figure 7. Operating CO_2 capacity of 8 m PZ and (7 and 11) m MEA assuming a 5 kPa rich CO_2 partial pressure at 40 °C (7 m and 11 m MEA data from Hilliard[12]).

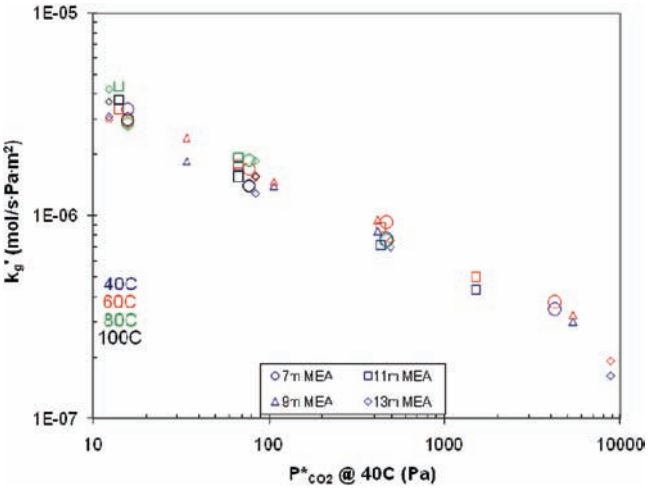

Figure 8. CO_2 absorption/desorption rates in MEA solutions at (40, 60, 80, and 100) °C, plotted against the 40 °C equilibrium CO_2 partial pressure.

CO_2 Mass Transfer Rate. The MEA data plotted in Figure 8 clearly show that the amine concentration and temperature do not significantly affect k_g' in MEA solutions over the range of conditions. It was surprising and unexpected that the amine concentration and temperature would not affect k_g' considering that the rate constant, free amine concentration, and diffusion coefficient of CO_2 are each strong functions of both temperature and amine concentration.

The measured k_g' values drastically decrease with increasing equilibrium CO_2 partial pressure at 40 °C (increasing CO_2 loading). The mass transfer coefficient decreases by about a factor of 10 from 0.25 to 0.50 CO_2 loading. The drop in k_g' is primarily due to the reduction of free MEA available for reaction.

Piperazine rate data at (40, 60, 80, and 100) °C are compared in Figure 9. PZ (12 m) data are not included since the equilibrium partial pressures could not be measured at 40 °C due to the high viscosity.

The PZ data converge similarly to the MEA data but with some outliers. k_g' seems independent of the total PZ concentration and

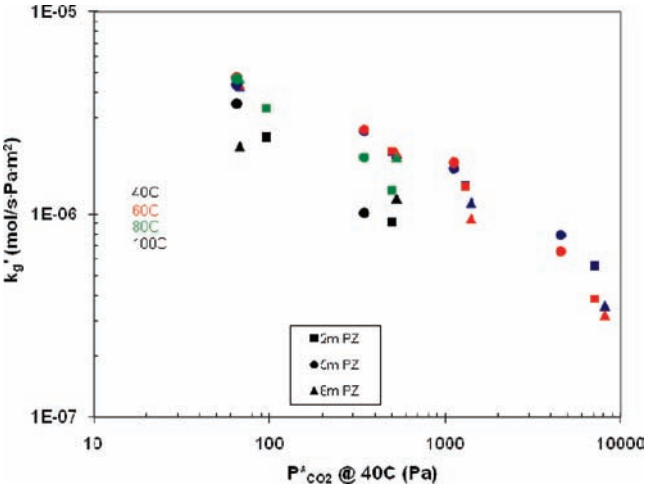

Figure 9. CO_2 absorption/desorption rates in PZ solutions at (40, 60, 80, and 100) °C, plotted against the 40 °C equilibrium CO_2 partial pressure.

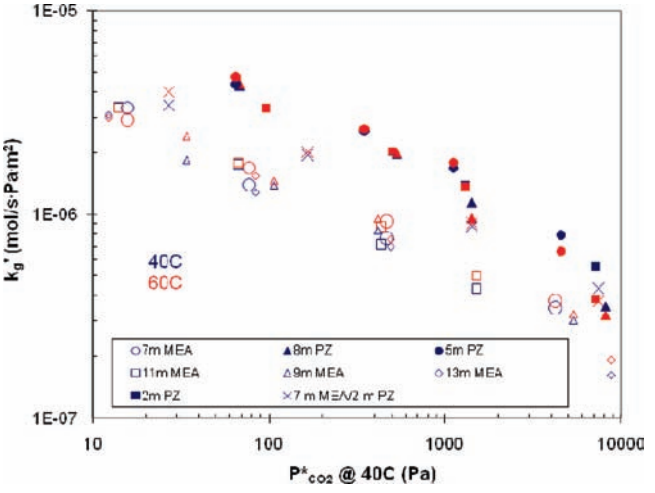

Figure 10. CO_2 absorption/desorption rates in MEA, PZ, and MEA/PZ solutions at (40 and 60) °C, plotted against the 40 °C equilibrium CO_2 partial pressure.

often the temperature. At the lowest CO_2 loading near (70 to 100) Pa, the 100 °C data points seem to drop below the trend of the other data. At the next higher CO_2 loading near (300 to 500) Pa, the 80 °C data points drop from the trend, while the 100 °C data points drop far below the trend. At the two highest loadings only (40 and 60) °C data are available, but the 60 °C data points routinely fall slightly below the 40 °C points.

The observed temperature effects in the PZ data suggest that diffusion of products and reactants may be limiting the reaction of the CO_2 with the amine. Tested CO_2 partial pressures range roughly from 0 to 2 times the equilibrium partial pressure, so fluxes are highest at higher temperatures and CO_2 loadings. There is also less free amine at higher CO_2 loading, increasing the possibility of a significant diffusion resistance.

The proposed diffusion limitation for the PZ experiments in the wetted wall column may not be seen in industrial columns. The wetted wall column has a smaller liquid film physical mass transfer coefficient, k_l^o, than a typical industrial column.

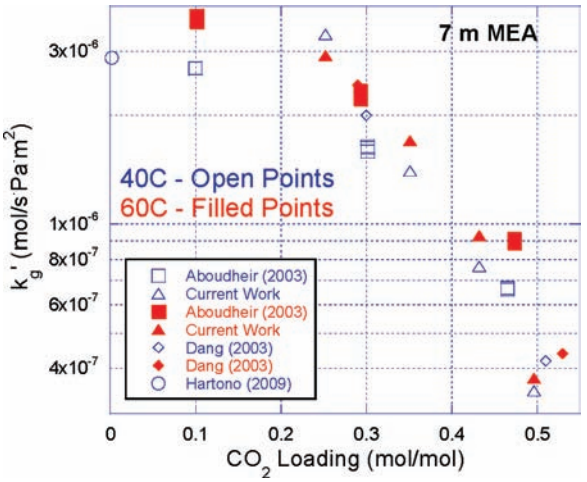

Figure 11. CO_2 reaction rate comparison on a k_g' basis for 7 m MEA at (40 and 60) °C.[3,4,6]

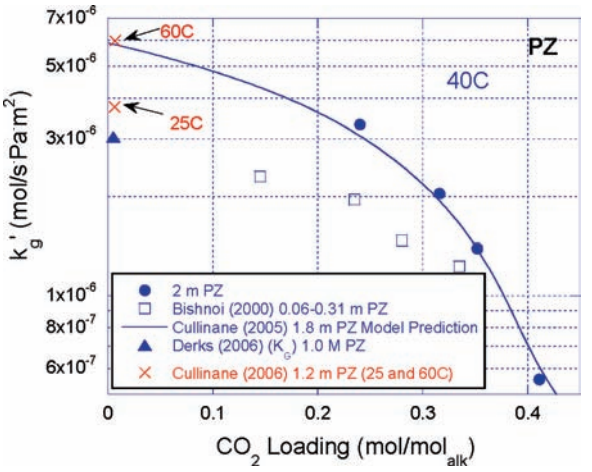

Figure 12. CO_2 reaction rate comparison on a k_g' basis for PZ solutions at 40 °C.[7,9,10,15]

The MEA, PZ, and MEA/PZ data are compared in Figure 10. MEA is represented by the empty points. PZ is represented by the filled data points. Data for 7 m MEA/2 m PZ are shown as ×'s.

Most of the PZ data points form a trend line above the MEA data. These data show that PZ is 2 to 3 times faster than MEA. The 7 m MEA/2 m PZ rate data generally fall between the MEA and PZ data.

Rate Comparisons with Literature. *Monoethanolamine Systems.* As previously stated, there are limited rate data on highly loaded concentrated amines. For a proper comparison on a k_g' basis, some raw data are required.

Figure 11 shows a comparison of 7 m MEA rate data at (40 and 60) °C. Aboudheir[3] provides rate data obtained from a laminar jet absorber. Figure 11 also includes four wetted wall column data points obtained by Dang.[4] Dang used the same wetted wall column used in this work. A single 40 °C data point from Hartono[6] is also included in Figure 11.

The data by Dang fit very nicely with the newly obtained wetted wall column data. The data by Aboudheir also fit nicely at the two higher CO_2 loadings. The data by Aboudheir[3] near 0.1 loading show a lower k_g' value than an extrapolation of the wetted wall column data would predict. However, the unloaded rate data by Hartono[6] support these 0.1 CO_2 loading values and suggest that the liquid film mass transfer coefficient, k_g', may not change significantly from 0 to 0.25 CO_2 loading.

The laminar jet absorber data by Aboudheir[3] seem to show a fairly reproducible effect of temperature. In each of the three CO_2 loadings, the 60 °C data points exhibit about 50 % higher k_g' values. The wetted wall column data including Dang[4] and the current work show a mostly negligible change in k_g' from (40 to 60) °C.

Piperazine Systems. Sun,[9] Derks,[11] Cullinane,[10] and Samanta[12] include unloaded PZ rate data, while Bishnoi[8] provides CO_2 loaded rate data. All five data sources use low piperazine concentrations. Due to various experimental methods and conditions, not all these data sources can be accurately compared to the obtained PZ rate data.

Derks uses a stirred cell and a "semi-continuous" gas phase operation. Numerous CO_2 partial pressures were tested for each amine to determine when the pseudofirst-order condition applies. At high CO_2 partial pressures, diffusion in the liquid phase limits CO_2 mass transfer. Inlet CO_2 partial pressures above 1.5 kPa showed a distinct effect of the partial pressure on the measured K_G. Below this threshold, the overall mass transfer coefficient is independent of the inlet partial pressure, and a pseudofirst-order k_g' can be obtained.

Sun[9] and Samanta[1] each measured the absorption into unloaded PZ solutions using wetted wall columns. However, each uses very high CO_2 partial pressures, typically about 5 kPa. At these high CO_2 partial pressures and amine concentrations below 1 M, CO_2 fluxes into the liquid phase are likely controlled by diffusion. In fact, Sun[9] tested a few lower CO_2 partial pressures, and these data verify that the system is not operating in the pseudofirst-order regime at the 5 kPa CO_2 pressure experiments, which comprise most of the data. A meaningful k_g' cannot be obtained from these data without quantifying the diffusion resistance via a model.

Cullinane provides all the required data to directly calculate k_g'. At each condition, five measurements were made. Obtained k_g' values were shown to range ± 30 % from the mean due to the high dependence of the gas film mass transfer coefficient. The 1.2 m PZ experiments were (54 to 73) % gas film controlled. Only (25 and 60) °C experiments were tested. The Cullinane experiments all use very low CO_2 partial pressures (<250 Pa), so the pseudofirst-order condition should apply.

Bishnoi[8] provides all of the data for a proper k_g' comparison but has only measured rates in very dilute piperazine.

Figure 12 shows a comparison of the obtained 2 m PZ wetted wall column rate data with literature obtained values. Figure 12 includes an unloaded 1.0 M PZ data point from Derks. This point is actually the obtained overall mass transfer, K_G, not the liquid film mass transfer coefficient, k_g'. Derks does not provide a gas film mass transfer coefficient correlation to quantify if or how much gas phase resistance limits CO_2 absorption into the solution. For purposes of comparison, the K_G obtained from Derks is plotted alongside the k_g' data and the k_g' model prediction from Cullinane.[16]

Figure 12 shows a good match of the current 2 m PZ rate data with the 1.8 m PZ model prediction by Cullinane.[16] The loaded Bishnoi data show mass transfer coefficients somewhat below the current data. This is expected due to the very low PZ concentration [(0.06 to 0.31) m PZ] in these experiments. Literature data generally show an effect of amine concentration at very low amine concentrations.[2]

dx.doi.org/10.1021/je101234t |*J. Chem. Eng. Data* 2011, 56, 2187–2195

The (25 and 60) °C data points by Cullinane show a significant temperature effect at 0 loading. These 1.2 m PZ data points show a decent fit to the 1.8 m 40 °C model prediction.

The Derks overall mass transfer coefficient falls significantly below the other unloaded data. This is expected considering stirred cell reactors generally have smaller gas film mass transfer coefficients than wetted wall columns. PZ (1.2 m) wetted wall column results from Cullinane[16] were (54 to 73) % gas film controlled. Stirred cell experiments are likely even more gas film controlled. It is likely that if the gas film resistance were removed from the overall mass transfer coefficient measured by Derks, the resulting k_g' would compare much more favorably with the other data.

CONCLUSIONS

At CO_2 loading less than 0.45 mol/mol alkalinity, the equilibrium CO_2 partial pressure in MEA is independent of amine concentration and depends only on temperature and CO_2. At greater loading, the CO_2 partial pressure increases with amine concentration in MEA.

With CO_2 loadings giving equilibrium CO_2 pressures of (100 and 5000) Pa at lean and rich conditions at 40 °C, the CO_2 capacity of 7 m MEA, 11 m MEA, and 8 m PZ is (0.85, 0.93, and 1.41) $mol_{CO2}/kg(water + amine)$.

The liquid film mass transfer coefficient, k_g', in aqueous MEA is essentially independent of temperature and the total amine concentration in the wetted wall column experiments. The CO_2 loading of the solution dictates k_g'. k_g' decreases by a factor of 30 in aqueous MEA with 0.23 to 0.50 CO_2 loading.

k_g' in aqueous PZ is independent of temperature and the total amine concentration at lower temperatures and CO_2 loading in the wetted wall column. Measured k_g' values are reduced at higher temperature and higher CO_2 loading. This phenomenon suggests a significant diffusion resistance in experiments at higher temperature and CO_2 loading. Industrial systems which possess larger physical mass transfer coefficients will not likely observe these depressed k_g' values. k_g' decreases by a factor of 20 in aqueous PZ with 0.21 to 0.41 CO_2 loading.

PZ absorbs CO_2 2 to 3 times faster than MEA and will require 2 to 3 times less absorber packing than MEA.

AUTHOR INFORMATION

Corresponding Author

*E-mail: gtr@che.utexas.edu.

Funding Sources

This work was made possible by financial support from the Luminant Carbon Management Program and the Industrial Associates Program for CO_2 Capture by Aqueous Absorption at the University of Texas.

NOMENCLATURE

A	Gas−liquid contact area
alk	Alkalinity (active nitrogen groups)
d	Hydraulic diameter
D_{CO2}	Diffusion coefficient of CO_2
g	Gravitational constant
h	Height of the contactor
K_G	Overall mass transfer coefficient (gas phase units) $(mol \cdot s^{-1} \cdot Pa^{-1} \cdot m^{-2})$
k_g	Gas film mass transfer coefficient $(mol \cdot s^{-1} \cdot Pa^{-1} \cdot m^{-2})$
k_g'	Liquid film mass transfer coefficient (gas phase units) $(mol \cdot s^{-1} \cdot Pa^{-1} \cdot m^{-2})$
k_g''	Pseudofirst-order liquid film mass transfer coefficient (gas phase units) $(mol \cdot s^{-1} \cdot Pa^{-1} \cdot m^{-2})$
k_l^o	Liquid film physical mass transfer coefficient $(m \cdot s^{-1})$
m	Molality (mol/kg_{H2O})
M	molarity $(mol \cdot L^{-1})$
MEA	Monoethanolamine
n	Moles
N_{CO2}	Flux of CO_2 $(mol \cdot s^{-1} \cdot m^{-2})$
$P^*_{CO2,b}$	Equilibrium CO_2 partial pressure of the bulk solution (Pa)
P_{CO2}	Partial pressure of CO_2 in the bulk gas (Pa)
$P_{CO2,i}$	Partial pressure of CO_2 at the gas−liquid interface (Pa)
PZ	Piperazine
Q	Solvent flow rate
R	Ideal gas constant
T	Temperature
Re	Reynolds number
Sc	Schmidt number
Sh	Sherwood number
SLPM	Standard liters per minute
x	Mole fraction with solution as total amine, total CO_2, and water
W	Circumference of the wetted wall column tube
μ	Viscosity
ρ	Density

REFERENCES

(1) Freeman, S. A.; Dugas, R. E.; Van Wagener, D. H.; Nguyen, T.; Rochelle, G. T. Carbon Dioxide Capture with Concentrated, Aqueous Piperazine. *Int. J. Greenhouse Gas Control* **2010**, *4*, 119–124.

(2) Versteeg, G. F.; Van Dijck, L. A. J.; Van Swaaij, W. P. M. On the Kinetics between CO_2 and Alkanolamines both in Aqueous and Non-aqueous Solutions. An Overview. *Chem. Eng. Commun.* **1996**, *144*, 113–158.

(3) Aboudheir, A.; Tontiwachwuthikul, P.; Chakma, A.; Idem, R. Kinetics of the reactive absorption of carbon dioxide in high CO_2-loaded, concentrated aqueous monoethanolamine solutions. *Chem. Eng. Sci.* **2003**, *58*, 5195–5210.

(4) Dang, H.; Rochelle, G. T. CO_2 Absorption Rate and Solubility in Monoethanolamine/Piperazine/Water. *Sep. Sci. Technol.* **2003**, *38*, 337–357.

(5) Jamal, A.; Meisen, A.; Lim, C. J. Kinetics of Carbon Dioxide Absorption and Desorption in Aqueous Alkanolamine Solutions Using a Novel Hemispherical Contactor - I. Experimental Apparatus and Mathematical Modeling. *Chem. Eng. Sci.* **2006**, *61*, 6571–6589.

(6) Hartono, A. Characterization of diethylenetriamine (DETA) as absorbent for CO2. *Ph.D. Dissertation*. Norwegian University of Science and Technology, Trondheim, Norway, 2009; p 243.

(7) Dugas, R.; Rochelle, G. Absorption and desorption rates of carbon dioxide with monoethanolamine and piperazine. *Energy Procedia* **2009**, *1*, 1163–1169.

(8) Bishnoi, S.; Rochelle, G. T. Absorption of Carbon Dioxide into Aqueous Piperazine: Reaction Kinetics, Mass Transfer and Solubility. *Chem. Eng. Sci.* **2000**, *55*, 5531–5543.

(9) Sun, W.-C; Yong, C.-B;Kinetics of the Absorption of Carbon Dioxide into Mixed Aqueous Alkanolamine Solutions of 2-amino-2-methyl-1-propanol and Piperazine. *Chem. Eng. Sci.* **2005**, *60*, 503–516.

(10) Cullinane, J. T.; Rochelle, G. T. Kinetics of Carbon Dioxide Absorption into Aqueous Potassium Carbonate and Piperazine. *Ind. Eng. Chem. Res.* **2006**, *45*, 2531–2545.

(11) Derks, P. W. J.; Kleingeld, T.; van Aken, C.; Hogendoorn, J. A.; Versteeg, G. F. Kinetics of Absorption of Carbon Dioxide in Aqueous Piperazine Solution. *Chem. Eng. Sci.* **2006**, *61*, 6837–6854.

(12) Samanta, A.; Bandyopadhyay, S. S. Kinetics and modeling of carbon dioxide into aqueous solutions of piperazine. *Chem. Eng. Sci.* **2007**, *62*, 7312–7319.

(13) Hilliard, M. A Predictive Thermodynamic Model for an Aqueous Blend of Potassium Carbonate, Piperazine, and Monoethanolamine for Carbon Dioxide Capture from Flue Gas. *Ph.D. Dissertation*, The University of Texas at Austin, 2008; p 1025.

(14) Davis, J. D. Thermal Degradation of Aqueous Amines Used for Carbon Dioxide Capture. *Ph.D. Dissertation*, The University of Texas at Austin, 2009; p 278.

(15) Mshewa, M. M. Carbon Dioxide Desorption/Absorption with Aqueous Mixtures of Methyldiethanolamine and Diethanolamine at 40 to 120 °C. *Ph.D. Dissertation*, The University of Texas at Austin, 1995.

(16) Cullinane, J. T. Thermodynamics and Kinetics of aqueous piperazine with potassium carbonate for carbon dioxide absorption. Ph.D. Dissertation, The University of Texas at Austin, 2005; p 295.

(17) Pacheco, M. A. Mass Transfer, Kinetics and Rate-Based Modeling of Reactive Absorption. *Ph.D. Dissertation*, The University of Texas at Austin, 1998; p 291.

(18) Al-Juaied, M.; Rochelle, G. T. Absorption of CO_2 in Aqueous Blends of Diglycolamine and Morpholine. *Chem. Eng. Sci.* **2006**, *61*, 3830–3837.

(19) Dugas, R. E. Carbon Dioxide Absorption, Desorption and Diffusion in Aqueous Piperazine and Monoethanolamine. Ph.D. Dissertation, The University of Texas at Austin, 2009; p 250.

(20) Jou, F.-Y.; Mather, A. E.; Otto, F. D. The Solubility of CO_2 in a 30 Mass Percent Monoethanolamine Solution. *Can. J. Chem. Eng.* **1995**, *73*, 140–147.

(21) Ermatchkov, V.; Perez-Salado Kamps, A.; Speyer, D.; Maurer, G. Solubility of Carbon Dioxide in Aqueous Solutions of Piperazine in the Low Gas Loading Region. *J. Chem. Eng. Data* **2006**, *51*, 1788–1796.

(22) Ermatchkov, V.; Perez-Salado Kamps, A.; Maurer, G. Solubility of Carbon Dioxide in Aqueous Solutions of N-Methyldiethanolaine in the Low Gas Loading Region. *Ind. Eng. Chem. Res.* **2006**, *45*, 6081–6091.

(23) Rochelle, G. T.; Chen, X. CO2 Capture by Aqueous Absorption - 1st Quarterly Progress Report 2009 from http://www.che.utexas.edu/rochelle_group/Pubs/Rochelle_Q1_Report_2009.pdf, 2009.